PHYSICAL REVIEW A **80**, 050702(R) (2009)

Intershell trielectronic recombination with *K*-shell excitation in Kr^{30+}

C. Beilmann,[1,*] O. Postavaru,[1] L. H. Arntzen,[1] R. Ginzel,[1] C. H. Keitel,[1] V. Mäckel,[1] P. H. Mokler,[1] M. C. Simon,[1] H. Tawara,[1] I. I. Tupitsyn,[1,2] J. Ullrich,[1] J. R. Crespo López-Urrutia,[1,†] and Z. Harman[1,3,‡]

[1]*Max-Planck-Institut für Kernphysik, Saupfercheckweg 1, 69117 Heidelberg, Germany*

[2]*St. Petersburg State University, Oulianovskaya 1, Petrovorets, 198504 St. Petersburg, Russia*

[3]*ExtreMe Matter Institute (EMMI), Planckstrasse 1, 64291 Darmstadt, Germany*

(Received 23 October 2008; published 4 November 2009)

We report the observation of trielectronic recombination with simultaneous excitation of a *K*-shell and an *L*-shell electron, hence involving three active electrons. This process was identified in the x-ray emission spectrum of recombining highly charged Kr ions. An energy resolution three times higher than any reported for this collision energy range around 10 keV resulted in the separation of the associated lines from the stronger dielectronic resonances. For Kr^{30+}, intershell trielectronic recombination contributions of nearly 6% to the total resonant photorecombination rate were found.

DOI: 10.1103/PhysRevA.80.050702 PACS number(s): 34.80.Lx, 31.30.jc, 32.80.Hd, 52.25.Os

Electron-electron interaction mediates the strongest atomic processes such as dielectronic recombination (DR) and its time reversal, Auger decay, following photoexcitation of an inner-shell electron [1,2]. Higher-order electron correlation plays also an essential role; however, these relevant processes are difficult to approach, both experimentally and theoretically. In the simple DR process involving only two interacting electrons, as sketched in Fig. 1 (left side), the kinetic energy of the recombined electron is transferred to a single bound electron by a radiationless excitation to an intermediate autoionizing state. The recombination is completed by its radiative stabilization. For the case of highly charged ions (HCIs), radiative transition probabilities are high, and the competition of radiative deexcitation and Auger decay of the intermediate state is biased toward the first mechanism.

Beyond the well-known DR, resonant recombination processes involving higher-order correlations are relevant, too. Here, as displayed in Fig. 1, two or even three bound electrons can be simultaneously excited by the resonantly captured electron in trielectronic or even quadruelectronic recombination (TR and QR, respectively).

Here, we present evidence for "intershell" TR involving excitation of a *K*-shell electron simultaneously with one of the *L* shells and provide a comparison with our theoretical predictions. TR and QR resonance energies and cross sections were predicted in the framework of the multiconfiguration Dirac-Fock (MCDF) method. Weak experimental signatures of intershell QR are also found at their calculated values. The processes we investigated are denoted as *KL-LLL* TR and *KLL-LLLL* QR, where the first set of capital letters indicates the initial shells of the bound electrons and the second one refers to the shells of the captured and excited electrons. In contrast to the already reported "intrashell" TR [3], for intershell higher-order processes the electron overlap is correspondingly smaller. Moreover, for higher atomic numbers the *e-e* correlation gets relatively weaker compared to the central force.

Resonant mechanisms are highly efficient in either ionizing or recombining ions and hence already DR is of paramount importance for the physics of outer planetary atmospheres and interstellar clouds as well as an important radiative cooling mechanism in astrophysical and laboratory high-temperature plasmas [1,2,4]. DR often represents the dominant pathway for populating excited states in plasmas and, consequently, for inducing easily observable x-ray lines which are used as diagnostic tools for fusion plasmas (whereby Kr as well as Ar were chosen as ideal candidates) [5,6], triggering a range of DR studies with highly charged Kr ions [7–9]. From a more fundamental point of view, the selectivity of DR [10] allows testing stringently sophisticated atomic structure and dynamics calculations, in particular of relativistic and quantum electrodynamic (QED) effects in bound electronic systems.

Investigating HCIs with DR offers additional important advantages including large cross sections and the magnification of relativistic and QED contributions by several orders of magnitude. These have been exploited in experiments both at electron beam ion traps (EBITs) (see, e.g., [11–16])

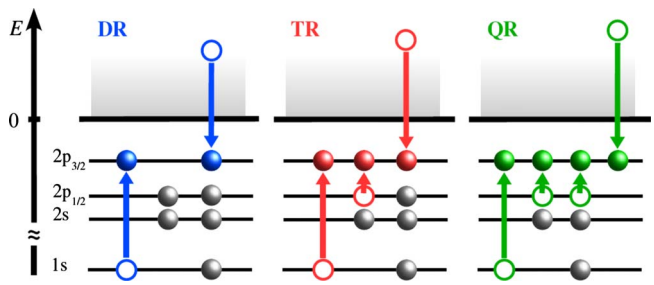

FIG. 1. (Color online) Scheme of resonant electron capture processes: in DR (left diagram) one bound electron is excited by the captured electron, in TR (middle diagram) two, and in QR (right diagram) three electrons are promoted by the captured electron (*K-LL*, *KL-LLL*, and *KLL-LLLL* processes, respectively, where the initial and the final shells of the bound and the active electrons are specified). The color code is used for all figures throughout this Rapid Communication.

*c.beilmann@mpi-hd.mpg.de
†j.crespo@mpi-hd.mpg.de
‡z.harman@mpi-hd.mpg.de

and in storage rings (SRs). The $2s_{1/2}$-$2p_{1/2}$ splitting in lithiumlike ions was determined in a SR with an accuracy capable of testing second-order QED corrections [10]. Direct EBIT spectroscopic measurements have achieved even higher precision [17]. Similarly, using DR in an ultracold electron target at a SR, the same splitting in Li-like Sc^{18+} has been indirectly determined with a precision of 4.6 ppm [18]. DR measurements have recently become sensitive to isotopic shifts in Li-like ^{142,150}Nd [19] and to the contribution of the generalized Breit interaction [16].

It is important to mention that in general TR and QR offer new photorecombination channels and their contributions to the radiative cooling of plasmas need to be considered in the theoretical modeling. However, very scarce experimental data are available. At interaction energies of less than 52 eV, intrashell TR resonances involving *L*-shell electrons of Cl^{13+} ions were observed at the TSR [3]. Contributions of roughly 10% to the total photorecombination rate at temperatures $T_e \approx 1-100$ eV (a range interesting for astrophysical photoionized plasmas) were found.

In collisionally excited plasmas at even higher temperatures, however, cooling by resonant recombination processes of higher order would be most effective when involving the far more energetic excitations of the *K* shell. An experiment reported in Ref. [20] was aimed at observing resonant electron transfer and double excitation in collisions of He-like Kr^{34+} ions with H_2 molecules. There, the two *K*-shell electrons should be excited by the quasi-free-electron captured from the light target molecules, but no clear signature could be found. Recent work using the ion-channeling technique could only determine an upper limit for the cross section of intershell TR processes with a double *K*-shell excitation in Kr^{34+} ions [21]. The time-reversed process of intershell TR, a three-electron Auger process in C^{3+} ions, was newly studied in a collision experiment [22]. Toward the next higher order, an observation of QR resonances has not been reported until now. However, other higher-order electron correlation processes have been reported earlier in electron-scattering experiments [23].

The higher-order recombination mechanisms can be summarized by the equation

$$A^{q+} + e^- \rightarrow [A^{(q-1)+}]^{(n+1)*} \rightarrow A^{(q-1)+} + (\text{photons}), \qquad (1)$$

where n represents the number of simultaneously excited bound electrons. The appearance of higher-order processes can be understood as follows: let us consider recombination of an electron of energy E with an initially C-like ion in its ground state, labeled by the dominant $|1s^2 2s^2 2p_{1/2}^2\rangle$ configuration. When describing TR, the autoionizing state can be approximated as a minimal linear combination of two configurations sharing total angular momentum and parity, $|\mathrm{TR}\rangle = c_1|1s2s^2 2p_{1/2} 2p_{3/2}^3\rangle + c_2|1s2s^2 2p_{1/2}^2 2p_{3/2}^2\rangle$. Here, the first term is the dominant one, as represented in the simplified scheme of Fig. 1. The neglect of the second term, i.e., the independent-particle (e.g., Hartree-Fock) approximation, would in the first order lead to a vanishing transition amplitude, $\langle 1s2s^2 2p_{1/2} 2p_{3/2}^3 | V_{Coul} | 1s^2 2s^2 2p_{1/2}^2 E\rangle = 0$. Only the inclusion of configuration mixing, a means of accounting for all-order electron correlation, leads to a non-vanishing amplitude $\langle \mathrm{TR}|V_{Coul}|1s^2 2s^2 2p_{1/2}^2 E\rangle = c_2\langle 1s2s^2 2p_{1/2}^2 2p_{3/2}^2|V_{Coul}|1s^2 2s^2 2p_{1/2}^2 E\rangle$. Thus, higher-order processes appear only if correlation effects are taken into account and their measurement can benchmark more thoroughly their theoretical description in terms of both structure and dynamics. In spite of their relevance, the exact quantitative description of such correlations and their scaling with the number of involved electrons remains an open theoretical problem.

The cross sections can be represented by a Lorentzian shape function centered at the resonance energy, given as the energy difference of the intermediate autoionizing state, denoted by $|d\rangle$, and the initial ionic state $|i\rangle$: $E_{res} = E_d - E_i$. The resonance strength observed at 90° is given as

$$S_{idf}^{DR} = \frac{\pi\hbar^3}{2p^2}\left(1 - \frac{\beta_{df}}{2}\right)\frac{2J_d + 1}{2(2J_i + 1)}\frac{A_r^{df} A_a^{di}}{\sum_f A_r^{df} + \sum_i A_a^{di}}. \qquad (2)$$

Here, p stands for the asymptotic momentum of the continuum electron and $|f\rangle$ is the state reached by one-photon decay of $|d\rangle$. *J* symbols denote the total angular momenta of the states, A_a^{di} denotes the autoionizing rate with the transition of n bound electrons including configuration mixing effects between DR and TR autoionizing states as described above, and A_r^{df} denotes the state-selective radiative decay rate. In Eq. (2), the dipole angular distribution factor for photon detection perpendicular to the electron beam direction was taken into account by means of the anisotropy parameter β_{df} [24]. Energies, their uncertainties, and wave functions of the bound states involved were determined by means of the MCDF method and by means of a configuration-interaction calculation as in [14]. QED terms were estimated by a semiempirical method accounting for electron screening. The uncertainties of the theoretical resonance energies are on the order of 5 eV. Continuum electron wave functions entering the two-, three-, or four-electron Auger rates are calculated with the screening potential induced by the bound frozen MCDF orbitals.

The experiment was performed at the Heidelberg EBIT [25] where highly charged Kr ions were produced and radially trapped by a 200 mA electron beam. A magnetic field of 8 T compresses the beam to a radius of ≈ 22 μm, calculated as in Ref. [26]. The ions were axially confined by electrostatic potentials applied to a set of drift tubes. The electron beam energy was swept in sawtooth ramps (2 V/s) over the expected range of resonance energies. This slow sweep rate maintained the HCI charge state distribution close to steady-state conditions. Photons emitted as signature of the direct and indirect photorecombinations and their cascades were detected with a high-purity germanium x-ray detector having a resolution of about 350 eV at 13 keV viewing the trap in a direction perpendicular to the exciting beam. The photons counted are represented in a two-dimensional intensity plot as a function of the electron beam energy. Bright spots at well-defined electron and photon energies reveal the recombination resonances in the illustration in Fig. 2. Projecting the counts within a certain photon energy region around the energy difference of the *K* and *L* shells (about 13 keV) onto the beam energy axis yields the energy-differential cross sec-

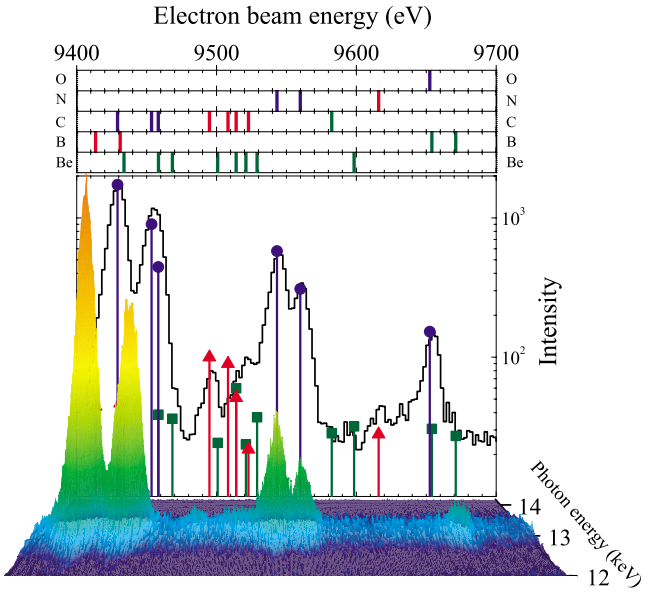

FIG. 2. (Color online) DR and TR resonances in the *K-LL* DR region of C- to O-like Kr ions as a projection and in three-dimensional illustration (photon intensity against electron beam and photon energies). Predictions (this work) for DR, TR, and QR resonances and their strengths are marked by blue circles, red triangles, and green squares (and corresponding lines), respectively. At the top the calculated resonances (color coded) for differently charged ion species are indicated.

tion of the photorecombination under perpendicular observation.

An excellent electron energy resolution of about 13 eV full width at half maximum at 10 keV was accomplished in our EBIT (a factor of 3 better in comparison to earlier experiments in any EBIT at these energies) and actually was prerequisite to resolve the weak peaks corresponding to intershell TR and separate them from the roughly 20 times stronger DR features. To achieve this, forced evaporative cooling of the ions in the trap [27] was optimized by lowering as much as possible the longitudinal trapping potential governing the ion escape by considering the trap generated by the space charge potential of the electron beam in dependence on the drift tube geometry as in Ref. [28]. In this way, the ion translational temperature was efficiently reduced, hence shrinking the range of the excursions of the ions in their motion around the trap axis. This improved ion confinement toward the radial potential minimum was found to be of crucial importance since the actual electron-ion interaction energy depends on the radial coordinate given that the space charge potential of the electron beam also does [28]. In contrast, the ion random kinetic energy only plays a minor role in the center-of-mass system.

Figure 2 presents an example of resonances appearing in electron energy scans of the C- to O-like *K-LL* DR region; well-resolved DR and TR resonances of C- to O-like Kr ions are found. Close to their theoretically expected positions, signatures of C- and Be-like intershell QR resonances are indicated as well.

Several measurements at different operation parameters consistently reproduced the TR resonances. Excitation energies were determined by adding all electron acceleration potentials. A space charge potential correction to the absolute energy scale was performed by referring it to the theoretical value of the strong C-like DR resonance at 9429 eV (theoretical uncertainty ±5 eV) with the intermediate state $[1s2s^22p_{1/2}^2(2p_{3/2}^2)_2]_{5/2}$ and calculating the small contribution of the energy-dependent part of that potential as in Ref. [28]. The experimental resonance energies for intershell TR as well as features which might be identified as signatures of QR are compared to the theoretical values in Table I. Our predictions agree very well within error bars with the intershell TR results and reasonably well with the weaker QR signatures.

TABLE I. Predicted and measured energies of selected dielectronic (DR), trielectronic (TR), and quadruelectronic (QR) resonances for Be-like to O-like Kr ions. The dominant autoionizing configurations are given in the *jj* coupling notation; subscripts following round brackets denote the angular momentum of coupled subshells and subscripts following square brackets stand for the total angular momentum of the level. The experimental errors correspond to statistical uncertainties. Proc. denotes the related process and CS refers to the charge state of the Kr ion.

Proc.	CS	Intermediate state	E_{expt} (eV)	E_{theor} (eV)
DR	C	$[1s2s^22p_{1/2}^2(2p_{3/2}^2)_2]_{5/2}$	9429.0(2)	9429(5)
DR	C	$[1s2s^22p_{1/2}^2(2p_{3/2}^2)_2]_{3/2}$	9455.0(3)	9455(5)
		$[1s2s^22p_{1/2}^2(2p_{3/2}^2)_0]_{1/2}$		
DR	N	$[1s2s^22p_{1/2}^22p_{3/2}^3]_2$	9543.9(3)	9543(6)
DR	N	$[1s2s^22p_{1/2}^22p_{3/2}^3]_1$	9561.6(4)	9560(6)
DR	O	$[1s2s^22p_{1/2}^22p_{3/2}^4]_{1/2}$	9653.8(4)	9653(7)
TR	C	$[(1s2s^22p_{1/2})_02p_{3/2}^3]_{3/2}$	9496.3(3)	9495(4)
TR	C	(blend)	9514.3(3)	9514(5)
TR	N	$[(1s2s^22p_{1/2})_12p_{3/2}^4]_1$	9617.5(7)	9616(6)
QR	Be	$[1s2p_{3/2}^4]_{1/2}$	9594(2)	9598(4)
QR	C	$[1s2s^22p_{3/2}^4]_{1/2}$	9576(2)	9582(4)

In Fig. 2 the theoretical resonance strengths were also normalized to the earlier mentioned C-like DR resonance line for Be-, B-, and C-like Kr and to the first corresponding DR line for N- and O-like ions. These values also show a good agreement with our predictions, thus further confirming the identification of the features as intershell TR resonances.

An overview of the calculated and measured DR, TR, and QR resonance strengths is shown in Fig. 3. The DR strength decreases monotonically with a growing number of L electrons. For intershell TR, the possible range of ion charges goes from the Li- to the N-like isoelectronic sequence. It is noteworthy that the predicted *KL-LLL* TR strength practically vanishes for initially Be-like ions due to parity reasons: while the TR resonances should necessarily be described by $|1s2s2p^3\rangle$ configurations possessing negative parity, the nearby *K-LL* DR configurations $|1s2s^22p^2\rangle$ are of positive parity, forbidding the requested admixtures. For this case, QR is the dominant higher-order recombination process. Interestingly, the ratio of intershell TR to the *total* DR resonance strength reaches values of up to 6% for C-like Kr^{30+}. This demonstrates that higher-order recombination processes

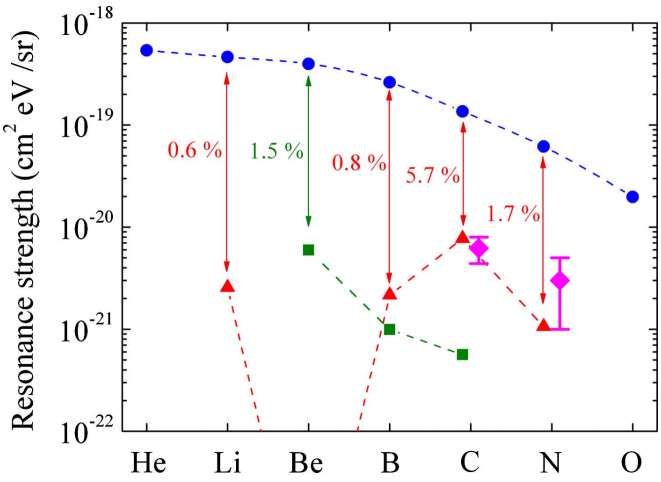

FIG. 3. (Color online) DR, TR, and QR resonances strengths for He- to O-like Kr ions. Theory: DR, blue circles; TR, red triangles; QR, green squares. Measured TR strength: magenta diamonds. The relative strengths of the higher-order recombination processes with respect to total DR are indicated.

of such mid-Z HCI contribute in the 1–10 % range to the total resonant photorecombination at interaction energies as high as 10 keV, which are relevant in the temperature range from $T_e = 500$ eV upward. The measured values confirm this statement. Experimental total TR resonance strengths of $(6.2 \pm 1.8) \times 10^{-21}$ cm^2 eV sr^{-1} for C-like and $(3 \pm 2) \times 10^{-21}$ cm^2 eV sr^{-1} for N-like ions agree reasonably well with theoretical values, as seen in Fig. 3. Moreover, they are remarkably large for a higher-order process in an intershell reaction involving a K-shell excitation. Studying HCIs at lower and higher Z values and, therefore, shifting from the nonrelativistic to the relativistic regime will help quantify these contributions for the benefit of fundamental understanding and of plasma physics applications.

In conclusion, *KL-LLL* trielectronic recombination in C- and N-like Kr ions was theoretically predicted. Simultaneously, it was observed in EBIT measurements, involving a K-shell electron as one of the actors. Furthermore, signatures of quadruelectronic resonances were found close to their expected positions; their unambiguous evaluation seems achievable in the near future. By investigating the electronic rearrangement taking place in such multiple excitations, another access to the study of entanglement and correlations of bound electrons is presented. The inclusion of these hitherto unexplored contributions raises the total resonant photorecombination x-ray yield by up to 6% at temperatures in the $T_e > 500$ eV range, an effect which has to be considered in the quantitative modeling of fusion and other hot, e.g., astrophysical plasmas. With the forced evaporative cooling technique applied, unprecedented resolution has been achieved for the recombination energies investigated. Future experimental improvements may even enable detailed studies of the hyperfine structure as well as of isotopic shifts.

This work was supported by Helmholtz Alliance HA216/EMMI.

[1] H. S. W. Massey and R. R. Bates, Rep. Prog. Phys. **9**, 62 (1942).
[2] A. Burgess, Astron. J. **139**, 886 (1964).
[3] M. Schnell *et al.*, Phys. Rev. Lett. **91**, 043001 (2003).
[4] S. A. Cohen *et al.*, J. Nucl. Mater. **176-177**, 909 (1990).
[5] J. Cummings *et al.*, J. Nucl. Mater. **176-177**, 916 (1990).
[6] K. Widmann *et al.*, Rev. Sci. Instrum. **66**, 761 (1995).
[7] M. Bitter *et al.*, Phys. Rev. Lett. **71**, 1007 (1993).
[8] T. Fuchs, C. Biedermann, R. Radtke, E. Behar, and R. Doron, Phys. Rev. A **58**, 4518 (1998).
[9] R. Radtke, C. Biedermann, T. Fuchs, G. Fussmann, and P. Beiersdorfer, Phys. Rev. E **61**, 1966 (2000).
[10] C. Brandau *et al.*, Phys. Rev. Lett. **91**, 073202 (2003).
[11] D. A. Knapp, P. Beiersdorfer, M. H. Chen, J. H. Scofield, and D. Schneider, Phys. Rev. Lett. **74**, 54 (1995).
[12] A. J. González Martínez *et al.*, Phys. Rev. Lett. **94**, 203201 (2005).
[13] A. J. González Martínez *et al.*, Phys. Rev. A **73**, 052710 (2006).
[14] Z. Harman *et al.*, Phys. Rev. A **73**, 052711 (2006).
[15] Y. Zou, J. R. Crespo López-Urrutia, and J. Ullrich, Phys. Rev. A **67**, 042703 (2003).
[16] N. Nakamura *et al.*, Phys. Rev. Lett. **100**, 073203 (2008).
[17] P. Beiersdorfer, H. Chen, D. B. Thorn, and E. Träbert, Phys. Rev. Lett. **95**, 233003 (2005).
[18] M. Lestinsky *et al.*, Phys. Rev. Lett. **100**, 033001 (2008).
[19] C. Brandau *et al.*, Phys. Rev. Lett. **100**, 073201 (2008).
[20] K. E. Zaharakis *et al.*, Phys. Rev. A **52**, 2910 (1995).
[21] M. Chevallier *et al.*, Phys. Rev. A **61**, 022724 (2000).
[22] E. De Filippo, G. Lanzano, H. Rothard, and C. Volant, Phys. Rev. Lett. **100**, 233202 (2008).
[23] A. Müller, K. Tinschert, G. Hofmann, E. Salzborn, and G. H. Dunn, Phys. Rev. Lett. **61**, 70 (1988).
[24] M. Gail, N. Grün, and W. Scheid, J. Phys. B **31**, 4645 (1998).
[25] J. R. Crespo López-Urrutia *et al.*, Phys. Scr. **T80**, 502 (1999).
[26] G. Herrmann, J. Appl. Phys. **29**, 127 (1958).
[27] B. M. Penetrante, J. N. Bardsley, M. A. Levine, D. A. Knapp, and R. E. Marrs, Phys. Rev. A **43**, 4873 (1991).
[28] B. M. Penetrante, J. N. Bardsley, D. DeWitt, M. Clark, and D. Schneider, Phys. Rev. A **43**, 4861 (1991).